ACS OMEGA

http://pubs.acs.org/journal/acsodf

Article

Room-Temperature Deep-UV Photoluminescence from Low-Dimensional Hexagonal Boron Nitride Prepared Using a Facile Synthesis

Ashly Sunny, Aniket Balapure, Ramakrishnan Ganesan, and R. Thamankar*

Cite This: *ACS Omega* 2022, 7, 33926−33933

Read Online

ACCESS | Metrics & More | Article Recommendations | Supporting Information

ABSTRACT: Identification and evaluation of defect levels in low-dimensional materials is an important aspect in quantum science. In this article, we report a facile synthesis method of low-dimensional hexagonal boron nitride (h-BN) and study light emission characteristics due to the defects. The thermal annealing procedure is optimized to obtain clean multilayered h-BN as revealed by transmission electron microscopy. UV−vis spectroscopy shows the optical energy gap of 5.28 eV, which is comparable to the reported energy gap for exfoliated, clean h-BN samples. X-ray photoelectron spectroscopy reveals the location of the valence band edge at 2 eV. The optimized synthesis route of h-BN generates two kinds of defects, which are characterized using room-temperature photoluminescence (PL) measurements. The defects emit light at 4.18 eV [deep-UV (DUV)] and 3.44 eV (UV) photons. The intensity of PL has an oscillatory dependence on the excitation energy for the defect emitting DUV light. A series of spectral lines are observed with the energy ranging between 2.56 and 3.44 eV. The average peak-to-peak energy separation is about 125 meV. The locations of the spectral lines can be modeled using Franck−Condon-type transition and associated with displaced harmonic oscillator approximation. Our facile route gives an easier approach to prepare clean h-BN, which is essential for classical two-dimensional material-based electronics and single-photon-based quantum devices.

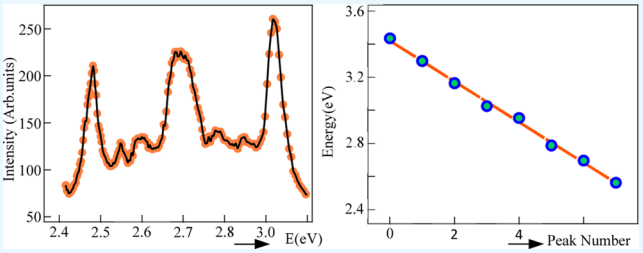

INTRODUCTION

Ever since graphene was exfoliated from graphite, curiosity in low-dimensional materials has been exponential and efforts in understanding the physics in low dimensions have regained importance.[1−3] Various low-dimensional materials have been studied, which are stable at room temperature.[4,5] Graphene as such lacks the electronic energy gap which is required in the electronic industry. MoS_2 is another two-dimensional (2D) material studied extensively in the last 2 decades which has an intrinsic electronic energy gap down to monolayers. A single layer of MoS_2 shows a direct energy gap of 1.8 eV and an indirect energy gap of 2 eV.[4,6,7] The electronic properties of MoS_2 are found to be layer-dependent, which gives an added advantage in using the material for hybrid applications. It is a well-established fact that the majority of these low-dimensional materials show a change in the electronic band structure with a number of layers, resulting in direct−indirect band gap transition. Since materials like MoS_2 can be exfoliated easily, much of the effort has been to use them in fabrication of nanoelectronic devices. Tremendous research has been done to use such monolayers to fabricate heterostructures with various other low-dimensional materials and thin films.[8,9] From no gap graphene to moderate energy gap materials such as MoS_2 and chalcogenides have been studied for a decade now.[10−13] Materials like monolayer MoS_2 and InSe show a direct band gap around 1.8 eV, while the energy gap reduces to a bulk value of about 1.2 −1.25 eV when measured for two to four monolayers.[6,14]

Recently, 2D wide band gap materials (E_g > 3 eV) have also attracted a lot of attention. Materials such as monolayer hexagonal boron nitride (h-BN) have attracted much attention due to their extremely large electronic energy gap (∼6 eV) and also stability at room temperature.[15−17] This promises to be used not only in the 2D material-based nanoelectronic devices but also as a platform for hosting useful defects. Materials like silicon carbide (SiC) and diamond (C) in the bulk have also attracted much attention due to their large band gap, which can host isolated defects energetically favorable as hosts for qubits.[18−21] There are theoretical first-principles calculations done on monolayer SiC showing the energy gap ranging between 2.5 and 2.8 eV.[22,23] Defect identification and analysis has been done using first principles and modeled under the

Received: May 9, 2022
Accepted: September 6, 2022
Published: September 15, 2022

Franck−Condon-type (FC-type) of spectrum using the harmonic oscillator approximation.[24]

In particular, h-BN has a layered structure similar to graphene. In view of this, h-BN can be considered as a versatile material for electronic devices. h-BN shows a hexagonal lattice with an alternative boron−nitrogen arrangement within the lattice, which is quite similar to the atomic arrangement of graphene. It is quite fascinating that even though h-BN and graphene (C) show similar atomic arrangements (the nearest neighbor distance, lattice parameters, and interlayer spacing), h-BN shows a large energy gap (∼6 eV), while "pure" graphene has no energy gap.[25]

A majority of studies performed on h-BN are by using bulk single crystals and mechanically exfoliating single to few layers of h-BN. Despite the extensive research performed on this material, the fundamental question about the energy gap remains still debatable.[26,27] The ab initio calculations and photoluminescence (PL) experiments give quite contrasting interpretations with large scatter in the values of the energy gap (E_g). While the ab initio calculations predict an indirect band gap, the optical measurements indicate a direct band gap.[28−32] The electronic band structure undergoes a crossover from an indirect band gap (bulk h-BN) to a direct band gap (monolayer h-BN).[33] In this context, it is essential to understand h-BN at monolayers in much detail. h-BN is a wide band gap layered material which hosts extremely bright-light-emitting defect centers stable at room temperature.[34,35] The defects present in h-BN emitting single photons have been studied recently. This is a primary requirement for single-photon-emitting sources and quantum photonics.[34,36−38] Theoretical investigations on monolayer h-BN reveal an overestimated wide energy gap compared to experimentally observed values. The energy gap calculated using density functional theory (DFT) calculations by the Bethe−Salpeter equation is more than 7 eV.[39,40] On the other hand, there are reports about calculations giving 6.47 eV using DFT−Vienna ab initio simulation package, yet there is no agreement between various procedures adopted in the calculations. Recently, experiments performed on h-BN/graphite using scanning tunneling microscopy/spectroscopy suggested an energy gap of 6.8 ± 0.2 eV.[41] The optical energy gap of monolayer h-BN has been determined using the exciton energy, and a range of energy gap values from 5.30 to 6.30 eV have been calculated.[39]

h-BN was also successfully synthesized using a variety of other techniques such as atomic layer deposition,[42] chemical vapor deposition,[43] molecular beam epitaxy,[33,44] and the layer-by-layer sputtering process.[45] Recently, large-area high-quality h-BN is grown on various substrates like sapphire and Ni(111) films, which is extremely important from the point of view of fabrication of devices for deep-UV (DUV) detection. Single-crystal domains as large as 0.6 mm have been observed on Ni(111)/sapphire(0001) films with such a synthesis route and show an optical energy gap of 5.76 eV.[46−48]

The low-dimensional wide band gap materials find their importance not only in the nanoscale transistor design but also for hosting the fundamental unit of quantum information processing, that is, qubit.[49] In this case, a two-level quantum system is idealized, and a transition between these two energy levels will emit a photon of a given wavelength. An ideal two-level system is provided by an isolated defect in 2D materials having a large energy gap. 2D systems which are structurally open, demonstrating the quantum confinement, and have reduced charge screening are ideal qualities for hosting the single-photon emitters. Since the electronic states of the single defect are well separated by the energy bands of the host lattice, it can be controlled by using the polarized light.[50,51] For example, the color centers in nanodiamonds are one such material platform which is stable and give good emission.[52] Similarly, the h-BN nanoparticles can host desirable defect centers which could be used in devices for quantum technologies. Interestingly, even a medium energy gap 2D material such as MoS_2 is also capable of hosting isolated defects. In a recently published article, it has been proved that sulfur defects can be prepared controllably using He-ion radiation, which act as single-photon emitters.[53] In essence, these defects are excellent candidates for quantum emission. The advancement in techniques used in miniaturization of electronic devices has led to conceive these atomic-scale devices using either atoms or molecules.

The possibility of using h-BN in the graphene-based transistor design is very promising. First, there is a good lattice match resulting in low-strained heterostructures, and h-BN showing a large band gap is essential as a dielectric in the transistor design. There have been numerous reports on the mechanism of dielectric breakdown of a few-layer h-BN using local breakdown studies. Notably, the nanoscale measurements using atomic force microscopy/spectroscopy are very crucial for understanding the fundamental mechanism of dielectric breakdown.[54]

For the synthesis of h-BN, boric acid ($B(OH)_3$) was used as a precursor for boron, whereas melamine ($C_3H_6N_6$) was used as a precursor for nitrogen. The original materials of boric acid powder ($B(OH)_3$, 99.95%) and melamine ($C_3H_6N_6$, 99.95%) were supplied by HiMedia Laboratories Pvt. Limited, India, and SDFCL (SD fine-Chem limited) India, respectively. The materials were of analytical grade and used as received without further purification. Boric acid is a weak, monobasic Lewis acid of boron. Boric acid exists in the form of colorless crystals or as a white powder that dissolves in water. Melamine is an organic compound which is a white solid and contains 67% nitrogen by mass.

We optimized a simple and facile procedure to synthesize multilayered h-BN. Herein, we report the fundamental analysis of prepared h-BN multilayers using X-ray diffraction (XRD), UV−vis spectroscopy, and X-ray photoelectron spectroscopy (XPS). Further, detailed PL studies were performed at room temperature to understand the defect energy levels and their light-emitting properties.

RESULTS AND DISCUSSION

Experimental Details. In a typical synthesis procedure shown in Figure 1, 8.15 g of boric acid and 1.84 g of melamine (in total, 10 g of the initial precursors by weight) were taken and mixed well using a mortar and pestle for 30 min and then transferred to a beaker containing methanol. This precursor mixture was ultrasonicated for 2 h and then dried at 70 °C, refer Figure 1c. Once the material completely dried, it was transferred to alumina boat and placed in a furnace under ambient conditions. We have tested various heating cycles considering the evolution of nitrogen from the melamine source and desorption of oxygen from the materials at different temperatures. The heating cycle which resulted in pure h-BN is shown in Figure 1b. The sample is heated at a rate of 6 °C/min to 400 °C and kept for 5 h. The melamine molecules partially dissociate into a nitrogen-rich precursor for h-BN. In the

https://doi.org/10.1021/acsomega.2c02884
ACS Omega 2022, 7, 33926−33933

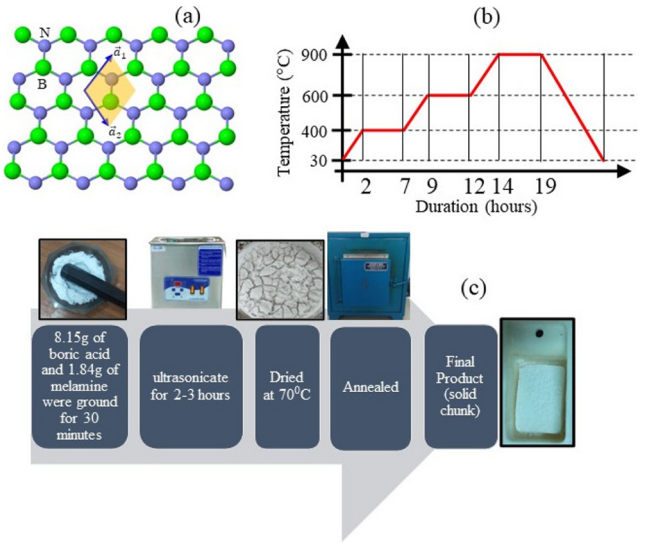

Figure 1. (a) Schematic diagram of 2D h-BN. Honeycomb structure of 2D h-BN with Bravais lattice vectors a_1 and a_2. The ball-stick model is represented by boron atoms (green) and nitrogen atoms (blue). (b) Optimized heat treatment involved in the synthesis of clean h-BN. Both the axes are not to the scale. (c) Synthetic route of preparing low-dimensional h-BN. The samples are annealed in a box furnace under ambient conditions. h-BN has the appearance of a bright white solid chunk.

second stage, the temperature is increased to 600 °C and maintained for 3 h. In this step, the boric acid partially dissociates to give rise to a boron-rich precursor for h-BN. In the third stage, the temperature is increased to 900 °C and maintained for 5 h. At this temperature, boron- and nitrogen-rich precursors react to give BN. The material is kept for sufficient duration to complete the reaction and then is allowed to cool down naturally to room temperature. The appearance of h-BN immediately taken out of the furnace is shown in Figure 1e, which appears as a white solid chunk. The actual reaction mechanism is shown in Figure S1 (Supporting Information).

The UV experiments were done on a Jasco V-670 UV−visible−NIR spectrometer. The sample was ultrasonicated for 2−3 h prior to the measurements and drop-cast onto a glass substrate and dried. Absorption and reflectance measurements were done on this sample. The reflectance spectrum was converted to the Kubelka−Munk function to calculate the optical band gap. PL experiments were done by dispersing the prepared and exfoliated sample in a solvent (DI water and methanol). The equipment used was a Cary Eclipse fluorescence spectrometer (G9800A). Initial scans were done for different excitation wavelengths (or energies), and emission spectra were observed in a broad wavelength range up to 1100 nm. Once the survey scan was taken, the excitation wavelength range was selected from 250 to 272 nm. For these values of excitation wavelengths, the sample showed a good emission spectrum with well-resolved peaks from 280 to 510 nm. Detailed scans were done in this range as it is of particular interest. The excitation wavelengths were varied with steps of 1 nm and scanned in the required range, and repeated measurements were done.

The phase purity and crystalline structure of the synthesized material were examined using XRD. We used Cu Kα_1 radiation with a wavelength of 1.5406 Å, and the data were collected from 10° to 90° (2θ) with a scanning rate of 2°/min. Figure 2 shows the XRD pattern obtained for the sample prepared with

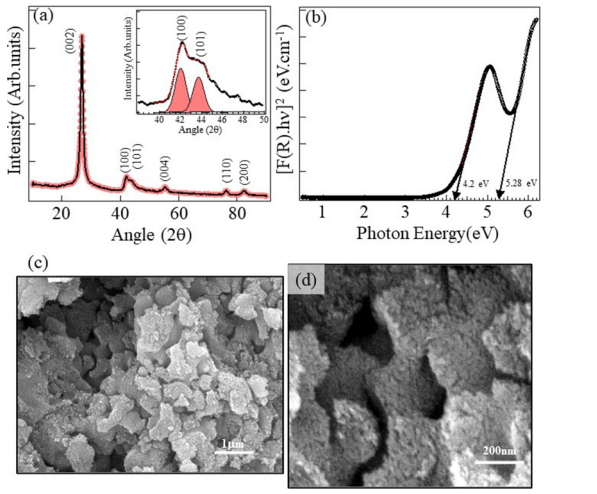

Figure 2. (a) Typical XRD pattern of multilayer h-BN. The principal reflection is at 26.8°, typical of the (200) reflection in h-BN. The inset in (a) shows peaks resolved appearing at 42°/43.7° showing (100)/101 reflections. (b) Kubelka−Munk plot to calculate the optical band gap. The two band edges corresponding to 5.28 and 4.2 eV are shown. (c,d) Large-area high-resolution scanning electron micrographs showing large-area h-BN. (c) Area is 6.83 μm × 5.00 μm and (d) area is 990 nm × 907 nm.

optimized annealing conditions. The principal diffraction peak is located at 2θ ∼ 26.9°, which is assigned for the (002) peaks of h-BN.[55,56] This peak pattern indicates that there is a similarity between graphite-like h-BN structures.

Further, much weaker peaks are observed at 42 and 43.7° attributed to (100)/(101), in close agreement with the reported values in the literature. The broad peaks at this position represent stacking faults in the (100) planes.[57] Such broad peaks are attributed to the "turbostatic" structure mentioned in the literature. However, the XRD peaks at this diffraction angle can be clearly resolved, which is close to h-BN, as shown in the inset of Figure 2a. Further, the peaks of [55.25°, (004)], [76.3°, (110)], and [82.4°, (200)] can also be identified in the large-angle diffraction. Such a narrow diffraction pattern is an indication of large-area h-BN layers. The interlayer spacing of the (200) crystallographic planes was calculated using Bragg's law, and we obtained a value of 0.331 nm, which is very close to the reported value of 0.333 nm for h-BN.[58] Corroborating our XRD analysis, the high-resolution electron microscopy images confirm large-area multilayers of h-BN. As shown in Figure 2c,d, large-area h-BN layers are formed. The high-resolution transmission electron microscopy images reveal either single-layer or few-layer h-BN as shown in Figure S2. At this point, efforts are underway to separate these sheets, resulting in single sheets.

The next step was to determine the optical band gap, and we used the standard UV−vis spectrometer to determine the absorbance and reflectance of the h-BN sample. We used reflectance to calculate the optical energy gap by means of the Kubelka−Munk function. As can be seen in Figure 2b, the calculated energy gap is about 5.28 eV, which agrees very well with the reported energy gap values.[59] It is to be noted that there is a large scatter in the determination of the optical band gap of h-BN in the literature. The energy gap measured in our

https://doi.org/10.1021/acsomega.2c02884
ACS Omega 2022, 7, 33926−33933

samples matches very well with the values obtained using the UV−vis spectrum available in the literature.[59] Additionally, we can also see a strong band of energy lying about 4.2 eV from the valence band edge. This is attributed to the defects which are discussed in detail in the later sections.

To find out the chemical nature of individual elements in h-BN multilayers, the survey scan and narrow-energy XPS scans were performed around the binding energies of boron (B), nitrogen (N), carbon (C), and oxygen (O). Global spectra of h-BN are shown in Figure 3a, which demonstrates a typical

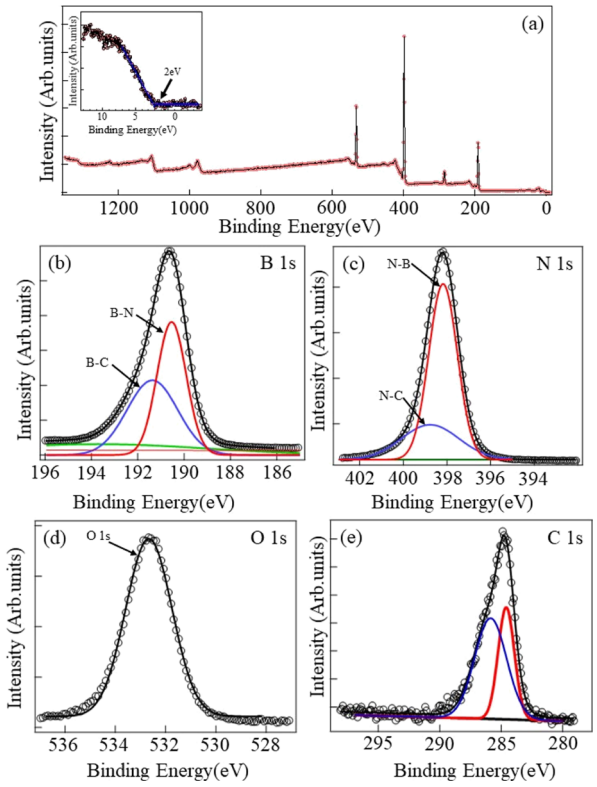

Figure 3. XPS measurements of h-BN samples. (a) Survey scan of the h-BN sample. The peaks for oxygen and carbon are denoted. The valence band maximum is shown in the inset. The line scans meet at 2 eV below the Fermi energy. (b) High-resolution scan of boron. The peak at 190.56 eV corresponds to B−N bonds, and the small shoulder at 191.56 eV corresponds to B−C bonds. (c) High-resolution N peak. The main peak is at 398.15 eV, which can be attributed to N−B bonds, and the shoulder at 399.2 eV can be attributed to N−C. (d) High-resolution peak at oxygen binding energy. (e) High-resolution C 1s peak at 284.59 eV and a shoulder at 285.56 eV.

spectrum with narrow peaks at various binding energy values characteristic of the high-quality sample. The survey scan depicts binding energy peaks at 190.56, 284.59, 398.15, and 532.64 eV corresponding to B (1s), C (1s), N (1s), and O (1s) from the h-BN sample, respectively. First, the valence band maximum (VBM) can be calculated by performing a high-resolution scan near the Fermi energy. As shown in the inset of Figure 3a, the VBM was calculated by considering the intersection of the flat XPS energy approaching the VB of h-BN and the linear fit of the VB edge in the XPS data. Such a calculation gives us the VBM at 2.0 eV below the Fermi energy. This is in very good agreement with the angle-resolved photoemission spectroscopy measurement on h-BN/(graphite), h-BN/Ir(111), and h-BN single crystals where the VBM has been found at 2.2−2.8 eV below the Fermi energy.[44] This implies that our facile synthesis method has resulted in very good quality h-BN. We take the binding energy of carbon (C 1s) at 284.59 eV as shown in the inset of Figure 3b as reference in all our analysis. The main peak is at 284.59 eV, arising from the sp^2 hybridization of carbon coming from the carbon support. The small shoulder peak arising at 285.56 eV can be attributed to C−O bonds, which could be from the adsorbed oxygen on the surface of h-BN.[60] The most dominant peak for boron is ∼190.56 eV, which is very close to the B−N bond value in h-BN.[61] This peak corresponds to the B−N bond in h-BN. The maximum intensity of the B−N peak at 190.56 eV shows the formation of the hexagonal phase of BN.[61−63] A small shoulder can be seen in higher energy at 191.56 eV, representing the B−C bond. Our inference is supported by the absence of B_2O_3 peaks in the XRD spectrum. The presence of B_2O_3 is shown by the strong XRD peak around $2\theta \sim 14.5°$.[64] Even though the survey scan shows a strong oxygen peak, it is not bonded to the boron atom, giving a B−O binding energy at 192 eV.[65] From this, it is clear that the oxygen peak shown in the full scan arises from the residual gas which is adsorbed on the surface.[66] As reported in the results from various groups, the enhanced peak at 532.8 eV attributed to the boron−oxygen bonding (corresponding to B_2O_3) is not seen in our sample, thereby reconfirming a complete h-BN phase formation in our sample. The high-resolution binding energy scan of nitrogen (N 1s) occurs at 398.15 eV, corresponding to the N−B bonding, and a small shoulder exists at 399.2 eV, which can be attributed to N−C bonds. Interestingly, the binding energy scan of oxygen shows a peak at 532.67 eV, which is due to the presence of B−O bonds. We assign this peak to the bond formation during ultrasonication of the h-BN layers. This can indicate the presence of numerous functional groups on the h-BN surface.

Careful analysis of the XPS spectrum and the binding energy position of various peaks reveal rich information about the defects present in h-BN. To support this, PL measurements have been a usual method employed to identify atomic-scale defects in h-BN.[16] Recently, using DFT, ab initio calculations, and core level binding energy calculations, the deconvoluted broad XPS spectrum positions were used to assign certain kinds of defects in the h-BN lattice.[67,68] Further, there are a variety of defects observed in h-BN such as a neutral nitrogen vacancy (V_N), a single-electron trapped nitrogen vacancy $(V_N)^{-1}$, a carbon atom replacing nitrogen (C_N), and some complex defects such as N_BV_N.[69−71] Most of the time, a nitrogen vacancy either neutral or singly occupied (V_N) is predominant in h-BN samples, which can be categorized as process-induced defects.

In order to check if our synthesis procedure resulted in such defects and decipher their light-emitting properties, room-temperature PL spectra were obtained on the prepared h-BN samples. As usual, the sample was excited using DUV light and the emission lines were checked. Since our sample contains single- or few-layer h-BN, we expected luminescence from various defect levels present in the sample. In particular, when excited with 265 nm (4.68 eV) photons, we achieved well-resolved PL spectra. The selection of the excitation wavelength (energy) is based on our Kubelka−Munk plot where we have seen an additional band edge at 4.2 eV (see Figure 2b). A typical PL spectrum is shown in Figure 4a. A series of emission lines varying in energy position can be seen. The first major peak appears at 361 nm (3.44 eV), followed by a series of

https://doi.org/10.1021/acsomega.2c02884
ACS Omega 2022, 7, 33926−33933

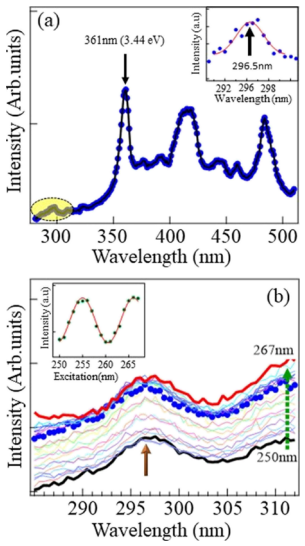

Figure 4. (a) Typical PL spectra of h-BN dispersed in water. The excitation wavelength is 265 nm. A series of defect-induced emission peaks are observed. The short-wavelength (DUV) emission is observed at 296.5 nm [4.18 eV, shaded region in (a)]. The inset in (a) shows a clear emission peak centered at 296.5 nm (4.18 eV). Major peaks at 361 nm (3.44 eV), 3.0−3.1 eV, and 2.56 eV shown in the figure show very high intensity. (b) Excitation wavelength dependence of intensity of the 296.5 nm (4.18 eV) peak. The black and red curves are the spectra obtained at 250 and 267 nm, respectively. The excitation wavelength of light is varied, and the intensity of 296.5 nm (4.18 eV) peak is monitored. The intensity shows a particular variation as shown in the inset (b).

variable intensity peaks. Since our main interest is to understand the additional band edge observed in the Kubelka−Munk plot, the scan range in PL is restricted to a small wavelength range up to 510 nm. First, we will discuss the PL spectra at lower wavelengths (DUV), as shown in Figure 4a (highlighted in yellow). For clarity, this is plotted in the inset of Figure 4a. The Gaussian fit of the data in this wavelength range shows intensity maximum at 296.5 nm (4.18 eV). This PL intensity is often attributed to the presence of carbon-substituted nitrogen (C_N) vacancies.[72] There are arguments about the origin of this peak due to intrinsic origin rather than extrinsic.[73] DFT within the LSDA and GGA shows that these levels are extended energy states close to the conduction band edge.[68] The calculations also suggest that the observed peak can also be from the boron vacancy (V_B). Even though we are not able to resolve this energy state at this moment, it strongly indicates that our sample preparation route has yielded very good h-BN samples. It should be noted that the intensity of the 296.5 nm (4.18 eV) peak is very small compared to the major peaks. The low intensity of this peak suggests that the overall PL intensity from our sample is not from the C_N but from other defects. A clearly resolved spectrum in these DUV and UV wavelength ranges is shown in Figure S3 (Supporting Information).

We measured the effect of excitation wavelength (energy) on this emission line. The wavelength was varied from 250 nm (4.96 eV) to 272 nm (4.55 eV), as shown in Figure 4b. The black to red curves represent the emission intensity for excitation at 250 nm (4.96 eV) to 272 nm (4.55 eV), respectively. Blue dotted spectra are for the excitation wavelength of 265 nm. The measured intensity variation of the 296.5 nm emission line with the excitation wavelength is plotted in the inset of Figure 4b. The intensity has an oscillatory dependence on excitation wavelength. Further studies are needed to elucidate such excitation energy dependence of emitted light. This variation can be seen as evidence for the bell-shaped energy levels/bands participating in the excitation and emission from the defects.[74] The intensity variation of all the measured spectra for various excitation wavelengths are plotted in Figure S3. It should be noted that intensity variation is not the same for all the peaks. In order to check if the emission lines observed are due to the solvent used, we performed the experiment using methyl alcohol (CH_3OH) as a solvent and compared the emission with that when water is used as a solvent. As shown in Figure S4 (Supporting Information), both emission spectra match very well, thus confirming that all the spectral lines discussed here are from h-BN.

To further analyze the spectrum shown in Figure 4a in the longer-wavelength regime (up to 510 nm), we convert the wavelength axis into energy (eV) and plot the PL intensity variation with the incident photon energy, as shown in Figure 5a. Apart from the DUV emitting center with very small

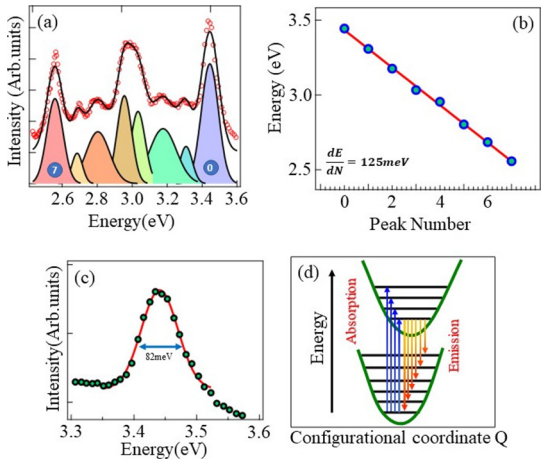

Figure 5. (a) PL spectra from h-BN dispersed in water as shown in Figure 4a with energy plotted along the *x*-axis. A series of defect-induced emission peaks are observed. These spectral peaks are satisfactorily fitted with Gaussian fitting as indicated from (0) to (7). (b) Energy positions of the peaks plotted against the peak number show that the average spacing between the peaks is ∼125 meV. (c) 3.44 eV is plotted for clarity. This peak shows a very good FWHM of ∼82 meV measured at room temperature. (d) Location of the spectral lines can be modeled using FC-type transition.

intensity, there are a series of emission lines in the energy range of 2.4−3.45 eV. The main feature of the series of lines is their closely lying spectral features. If one observes Figure 5a, one can note that there are three strong resonances at 3.45 eV, a broad peak at 3.025 eV, and a sharp peak at 2.56 eV. We used the Gaussian peak fitting for each peak as shown by the colored Gaussian noted with numbers from 0 to 7. Overall intensity variation can be satisfactorily explained with this fitting, as indicated by the black spectral curve. All peaks do not show the same intensity and full width at half-maximum (FWHM) values. If one plots the peak energy positions, it falls on a straight line as shown in Figure 5b. The average peak-to-peak separation is about 125 meV, as shown in Figure 5b.[75,76] The measured peak positions, the relative peak position with respect to 3.45 eV, and the FWHM of each spectral line are

https://doi.org/10.1021/acsomega.2c02884
ACS Omega 2022, 7, 33926−33933

Table 1. Energetic Position of Spectral Lines[a]

peak number	0	1	2	3	4	5	6	7
peak location (eV)	3.44	3.30	3.16	3.03	2.95	2.79	2.70	2.56
relative peak position with respect to 3.44 eV	0	−0.13	−0.26	−0.40	−0.47	−0.64	−0.73	−0.86
FWHM (eV)	0.115	0.093	0.180	0.097	0.099	0.157	0.072	0.111

[a]The measured energy position, the relative energy position with respect to 3.44 eV, and the FWHM of all peaks are also shown.

shown in Table 1. The series of spectral lines are resonances related to single defects. The defect shows up like a harmonic oscillator when an excited electron undergoes a vibrational transition into a higher energy level. During the de-excitation to the ground state, a series of spectral lines are observed. A similar observation has been made on substitutional nitrogen impurity close to silicon vacancy in SiC.[24] It has been shown that the PL from the defect centers can be modeled using FC-type defects with displaced harmonic oscillator approximation, and the series of spectral lines associated can be attributed to the phonon bands. There are reports on PL from few-layer h-BN that the series of detuned spectral lines can be associated to the emission of acoustic phonons assisted radiative recombination with detuning less than 150 meV.[77] Our measurements could indicate a similar situation of a defect-induced emission band with a 3.45 eV peak as the main spectral line.

CONCLUSIONS

Understanding the defect structure in h-BN paves the way to fabricate single-photon sources with well-defined emission wavelengths. The synthesis of such a photon source should be easy and cost-effective. Here, multilayer h-BN is prepared using a facile synthesis method which involves heating the precursors in a controlled manner under ambient conditions. A detailed analysis of the XRD pattern reveals that the optimized heating procedure indeed yields clean h-BN. Further, the UV−vis spectra show an energy gap (5.28 eV) comparable to the reported values in literature. The process-induced defects show light emission in the DUV region, which is also very essential for the quantum communication in the DUV region. We find two types of defects in our samples emitting DUV light at 4.18 eV, which indicates a well-studied carbon-substituted nitrogen vacancy (C_N), and UV light at 3.44 eV. We attribute the defect emitting 3.44 eV photons to the nitrogen vacancies created during the synthesis of h-BN. The defect emission at 3.44 eV shows a very sharp spectral line even at room temperature. The harmonic oscillator approximation is utilized to understand the series of spectral lines shown very close to 3.44 eV, and the energy level separation is found to be about 125 meV at room temperature. Our synthesis method is an easy-to-do route to prepare high-quality h-BN with deep UV-emitting defects which are useful in the DUV photonic applications and quantum computation.

ASSOCIATED CONTENT

Supporting Information

The Supporting Information is available free of charge at https://pubs.acs.org/doi/10.1021/acsomega.2c02884.

Reaction scheme of h-BN preparation; transmission electron microscopy images of h-BN; excitation wavelength dependance of PL at the lower-wavelength region; and emission spectra using the two solvents H_2O and CH_3OH (PDF)

AUTHOR INFORMATION

Corresponding Author

R. Thamankar − *Centre for Functional Materials, Vellore Institute of Technology, Vellore, Tamilnadu 632014, India;* orcid.org/0000-0002-1761-1970; Phone: +91 9742430830; Email: rameshm.thamankar@vit.ac.in

Authors

Ashly Sunny − *Department of Physics, School of Advanced Sciences, Vellore Institute of Technology, Vellore 632014, India*

Aniket Balapure − *Department of Chemistry, Birla Institute of Technology and Science (BITS), Hyderabad, Telangana 500078, India*

Ramakrishnan Ganesan − *Department of Chemistry, Birla Institute of Technology and Science (BITS), Hyderabad, Telangana 500078, India;* orcid.org/0000-0003-4122-3174

Complete contact information is available at: https://pubs.acs.org/10.1021/acsomega.2c02884

Notes

The authors declare no competing financial interest.

ACKNOWLEDGMENTS

A.S. and R.T. would like to thank Vellore Institute of Technology for their support during this research work. R.T. acknowledges the support of Dr. R.G. from BITS Hyderabad for the XPS measurements. R.T. acknowledges the HRTEM FACILITY at SRMIST setup with support from MNRE (project no. 31/03/2014−15/PVSE-R&D), Government of India. R.T. would like to acknowledge Dr. Rajagopal Desikan, Department of Chemistry, VIT Vellore, for critical reading of the manuscript.

REFERENCES

(1) Neto, A. H. C.; Guinea, F.; Peres, N. M. R.; Novoselov, K. S.; Geim, A. K. The electronic properties of graphene. *Rev. Mod. Phys.* **2009**, *81*, 109.

(2) Novoselov, K.; Geim, A.; Morozov, S.; Jiang, D.; Zhang, Y.; Dubonos, S.; Grigorieva, I.; Firsov, A. Electric Field Effect in Atomically Thin Carbon Films. *Science* **2004**, *306*, 666.

(3) Geim, A.; Novoselov, K. The rise of graphene. *Nat. Mater.* **2007**, *6*, 183.

(4) Mak, K. F.; Lee, C.; Hone, J.; Shan, J.; Heinz, T. F. Atomically Thin MoS_2: A New Direct-Gap Semiconductor. *Phys. Rev. Lett.* **2010**, *105*, 136805.

(5) Bhimanapati, G. R.; Lin, L.; Meunier, V.; Jung, J.; Cha, C.; Das, S.; Xiao, D.; Son, Y.; Strano, M. S.; Cooper, L.; et al. Recent Advances in Two-Dimensional Materials beyond Graphene. *ACS Nano* **2015**, *9*, 11509.

(6) Splendiani, A.; Sun, L.; Zhang, Y.; Li, T.; Kim, J.; Chim, C. Y.; Galli, G.; Wang, F. Emerging Photoluminescence in Monolayer MoS2. *Nano Lett.* **2010**, *10*, 1271.

(7) Eda, G.; Yamaguchi, H.; Voiry, D.; Fujita, T.; Chen, M.; Chhowalla, M. Photoluminescence from Chemically Exfoliated MoS2. *Nano Lett.* **2011**, *11*, 5111.
(8) Novoselov, K. S.; Mishchenko, A.; Carvalho, A.; Castro Neto, A. H. 2D materials and van der Waals heterostructures. *Science* **2016**, *353*, aac9439.
(9) Gibertini, M.; Koperski, M.; Morpurgo, A. F.; Novoselov, K. S. Magnetic 2D materials and heterostructures. *Nat. Nanotechnol.* **2019**, *14*, 408.
(10) Radisavljevic, B.; Radenovic, A.; Brivio, J.; Giacometti, V.; Kis, A. Single-layer MoS2 transistors. *Nat. Nanotechnol.* **2011**, *6*, 147.
(11) Castellanos-Gomez, A.; Cappelluti, E.; Roldán, R.; Agraït, N.; Guinea, F.; Rubio-Bollinger, G. Electric-Field Screening in Atomically Thin Layers of MoS2: the Role of Interlayer Coupling. *Adv. Mater.* **2013**, *25*, 899.
(12) Wang, Q. H.; Kalantar-Zadeh, K.; Kis, A.; Coleman, J. N.; Strano, M. S. Electronics and optoelectronics of two-dimensional transition metal dichalcogenides. *Nat. Nanotechnol.* **2012**, *7*, 699.
(13) Sangwan, V. K.; Hersam, M. C. Electronic Transport in Two-Dimensional Materials. *Annu. Rev. Phys. Chem.* **2018**, *69*, 299.
(14) Sun, Y.; Luo, S.; Zhao, X.-G.; Biswas, K.; Li, S.-L.; Zhang, L. InSe: a two-dimensional material with strong interlayer coupling. *Nanoscale* **2018**, *10*, 7991.
(15) Kubota, Y.; Watanabe, K.; Tsuda, O.; Taniguchi, T. Deep Ultraviolet Light-Emitting Hexagonal Boron Nitride Synthesized at Atmospheric Pressure. *Science* **2007**, *317*, 932.
(16) Museur, L.; Feldbach, E.; Kanaev, A. Defect-related photoluminescence of hexagonal boron nitride. *Phys. Rev. B: Condens. Matter Mater. Phys.* **2008**, *78*, 155204.
(17) Watanabe, K.; Taniguchi, T. Hexagonal Boron Nitride as a New Ultraviolet Luminescent Material and Its Application. *Int. J. Appl. Ceram. Technol.* **2011**, *8*, 977.
(18) Baranov, P. G.; Bundakova, A. P.; Soltamova, A. A.; Orlinskii, S. B.; Borovykh, I. V.; Zondervan, R.; Verberk, R.; Schmidt, J. Silicon vacancy in SiC as a promising quantum system for single-defect and single-photon spectroscopy. *Phys. Rev. B: Condens. Matter Mater. Phys.* **2011**, *83*, 125203.
(19) Koehl, W. F.; Buckley, B. B.; Heremans, F. J.; Calusine, G.; Awschalom, D. D. Room temperature coherent control of defect spin qubits in silicon carbide. *Nature* **2011**, *479*, 84.
(20) Balasubramanian, G.; Neumann, P.; Twitchen, D.; Markham, M.; Kolesov, R.; Mizuochi, N.; Isoya, J.; Achard, J.; Beck, J.; Tissler, J.; et al. Ultralong spin coherence time in isotopically engineered diamond. *Nat. Mater.* **2009**, *8*, 383.
(21) Dzurak, A. Diamond and silicon converge. *Nature* **2011**, *479*, 47−48.
(22) Shi, Z.; Zhang, Z.; Kutana, A.; Yakobson, B. I. Predicting Two-Dimensional Silicon Carbide Monolayers. *ACS Nano* **2015**, *9*, 9802.
(23) Şahin, H.; Cahangirov, S.; Topsakal, M.; Bekaroglu, E.; Akturk, E.; Senger, R. T.; Ciraci, S. Monolayer honeycomb structures of group-IV elements and III-V binary compounds: First-principles calculations. *Phys. Rev. B: Condens. Matter Mater. Phys.* **2009**, *80*, 155453.
(24) Jin, Y.; Govoni, M.; Wolfowicz, G.; Sullivan, S. E.; Heremans, F. J.; Awschalom, D. D.; Galli, G. Photoluminescence spectra of point defects in semiconductors: Validation of first-principles calculations. *Phys. Rev. Mater.* **2021**, *5*, 084603.
(25) Pakdel, A.; Zhi, C.; Bando, Y.; Golberg, D. Low-dimensional boron nitride nanomaterials. *Mater. Today* **2012**, *15*, 256.
(26) Cassabois, G.; Valvin, P.; Gil, B. Hexagonal boron nitride is an indirect bandgap semiconductor. *Nat. Photonics* **2016**, *10*, 262.
(27) Watanabe, K.; Taniguchi, T.; Kanda, H. Direct-bandgap properties and evidence for ultraviolet lasing of hexagonal boron nitride single crystal. *Nat. Mater.* **2004**, *3*, 404−409.
(28) Xu, Y.-N.; Ching, W. Y. Calculation of ground-state and optical properties of boron nitrides in the hexagonal, cubic, and wurtzite structures. *Phys. Rev. B: Condens. Matter Mater. Phys.* **1991**, *44*, 7787−7798.
(29) Furthmüller, J.; Hafner, J.; Kresse, G. Ab initio calculation of the structural and electronic properties of carbon and boron nitride using ultrasoft pseudopotentials. *Phys. Rev. B: Condens. Matter Mater. Phys.* **1994**, *50*, 15606−15622.
(30) Blase, X.; Rubio, A.; Louie, S. G.; Cohen, M. L. Quasiparticle band structure of bulk hexagonal boron nitride and related systems. *Phys. Rev. B: Condens. Matter Mater. Phys.* **1995**, *51*, 6868−6875.
(31) Arnaud, B.; Lebègue, S.; Rabiller, P.; Alouani, M. Huge excitonic effects in layered hexagonal boron nitride. *Phys. Rev. Lett.* **2006**, *96*, 026402.
(32) Evans, D. A.; McGlynn, A. G.; Towlson, B. M.; Gunn, M.; Jones, D.; Jenkins, T. E.; Winter, R.; Poolton, N. R. J. Determination of the optical band-gap energy of cubic and hexagonal boron nitride using luminescence excitation spectroscopy. *J. Phys. Condens. Matter* **2008**, *20*, 075233.
(33) Elias, C.; Valvin, P.; Pelini, T.; Summerfield, A.; Mellor, C. J.; Cheng, T. S.; Eaves, L.; Foxon, C. T.; Beton, P. H.; Novikov, S. V.; et al. Direct band-gap crossover in epitaxial monolayer boron nitride. *Nat. Commun.* **2019**, *10*, 2639.
(34) Tran, T. T.; Bray, K.; Ford, M. J.; Toth, M.; Aharonovich, I. Quantum emission from hexagonal boron nitride monolayers. *Nat. Nanotechnol.* **2016**, *11*, 37.
(35) Tran, T. T.; Elbadawi, C.; Totonjian, D.; Lobo, C. J.; Grosso, G.; Moon, H.; Englund, D.; Ford, M. J.; Aharonovich, I.; Toth, M. Robust Multicolor Single Photon Emission from Point Defects in Hexagonal Boron Nitride. *ACS Nano* **2016**, *10*, 7331.
(36) Toth, M.; Aharonovich, I. Single Photon Sources in Atomically Thin Materials. *Annu. Rev. Phys. Chem.* **2019**, *70*, 123.
(37) Gil, B.; Cassabois, G.; Cusco, R.; Fugallo, G.; Artus, L. Boron nitride for excitonics, nano photonics and quantum technologies. *Nanophotonics* **2020**, *9*, 3483−3504.
(38) Exarhos, A. L.; Hopper, D. A.; Patel, R. N.; Doherty, M. W.; Bassett, L. C. Magnetic-field-dependent quantum emission in hexagonal boron nitride at room temperature. *Nat. Commun.* **2019**, *10*, 222.
(39) Ferreira, F.; Chaves, A. J.; Peres, N. M. R.; Ribeiro, R. M. Excitons in hexagonal boron nitride single-layer: a new platform for polaritonics in the ultraviolet. *J. Opt. Soc. Am. B* **2019**, *36*, 674−683.
(40) Ba, K.; Jiang, W.; Cheng, J.; Bao, J.; Xuan, N.; Sun, Y.; Liu, B.; Xie, A.; Wu, S.; Sun, Z. Chemical and Bandgap Engineering in Monolayer Hexagonal Boron Nitride. *Sci. Rep.* **2017**, *7*, 45584.
(41) Román, R. J. P.; Costa, F. J. R. C.; Zobelli, A.; Elias, C.; Valvin, P.; Cassabois, G.; Gil, B.; Summerfield, A.; Cheng, T. S.; Mellor, C. J.; et al. Band gap measurements of monolayer h-BN and insights into carbon-related point defects. *2D Mater.* **2021**, *8*, 044001.
(42) Park, H.; Kim, T.; Cho, S. W.; Jang, H. S.; Lee, S.; Choi, S.-Y. Large-scale synthesis of uniform hexagonal boron nitride films by plasma-enhanced atomic layer deposition. *Sci. Rep.* **2017**, *7*, 40091.
(43) Kim, K. K.; Hsu, A.; Jia, X.; Kim, S. M.; Shi, Y.; Hofmann, M.; Nezich, D.; Rodriguez-Nieva, J. F.; Dresselhaus, M.; Palacios, T.; et al. Synthesis of Monolayer Hexagonal Boron Nitride on Cu Foil Using Chemical Vapor Deposition. *Nano Lett.* **2012**, *12*, 161−166.
(44) Pierucci, D.; Zribi, J.; Henck, H.; Chaste, J.; Silly, M. G.; Bertran, F.; Le Fevre, P.; Gil, B.; Summerfield, A.; Beton, P. H.; et al. Van der Waals epitaxy of two-dimensional single-layer h-BN on graphite by molecular beam epitaxy: Electronic properties and band structure. *Appl. Phys. Lett.* **2018**, *112*, 253102.
(45) Jin, C.; Lin, F.; Suenaga, K.; Iijima, S. Fabrication of a Freestanding Boron Nitride Single Layer and Its Defect Assignments. *Phys. Rev. Lett.* **2009**, *102*, 195505.
(46) Chen, J.; Wang, G.; Meng, J.; Cheng, Y.; Yin, Z.; Tian, Y.; Huang, J.; Zhang, S.; Wu, J.; Zhang, X. Low-Temperature Direct Growth of Few-Layer Hexagonal Boron Nitride on Catalyst-Free Sapphire Substrates. *ACS Appl. Mater. Interfaces* **2022**, *14*, 7004.
(47) Gao, M.; Meng, J.; Chen, Y.; Ye, S.; Wang, Y.; Ding, C.; Li, Y.; Yin, Z.; Zeng, X.; You, J.; et al. Catalyst-free growth of two-dimensional hexagonal boron nitride few-layers on sapphire for deep ultraviolet photodetectors. *J. Mater. Chem. C* **2019**, *7*, 14999.

https://doi.org/10.1021/acsomega.2c02884
ACS Omega 2022, 7, 33926−33933

(48) Meng, J.; Zhang, X.; Wang, Y.; Yin, Z.; Liu, H.; Xia, J.; Wang, H.; You, J.; Jin, P.; Wang, D.; et al. Aligned Growth of Millimeter-Size Hexagonal Boron Nitride Single-Crystal Domains on Epitaxial Nickel Thin Film. *Small* **2017**, *13*, 1604179.
(49) Weber, J. R.; Koehl, W. F.; Varley, J. B.; Janotti, A.; Buckley, B. B.; Van de Walle, C. G.; Awschalom, D. D. Quantum computing with defects. *Proc. Natl. Acad. Sci.* **2010**, *107*, 8513.
(50) Gupta, S.; Yang, J. H.; Yakobson, B. I. Two-Level Quantum Systems in Two-Dimensional Materials for Single Photon Emission. *Nano Lett.* **2019**, *19*, 408−414.
(51) Frey, N. C.; Akinwande, D.; Jariwala, D.; Shenoy, V. B. Machine Learning-Enabled Design of Point Defects in 2D Materials for Quantum and Neuromorphic Information Processing. *ACS Nano* **2020**, *14*, 13406−13417.
(52) Wolters, J.; Schell, A. W.; Kewes, G.; Nüsse, N.; Schoengen, M.; Döscher, H.; Hannappel, T.; Löchel, B.; Barth, M.; Benson, O. Enhancement of the zero phonon line emission from a single nitrogen vacancy center in a nanodiamond via coupling to a photonic crystal cavity. *Appl. Phys. Lett.* **2010**, *97*, 141108.
(53) Klein, J.; Sigl, L.; Gyger, S.; Barthelmi, K.; Florian, M.; Rey, S.; Taniguchi, T.; Watanabe, K.; Jahnke, F.; Kastl, C.; et al. Engineering the Luminescence and Generation of Individual Defect Emitters in Atomically Thin MoS_2. *ACS Photonics* **2021**, *8*, 669−677.
(54) Ranjan, A.; Raghavan, N.; Holwill, M.; Watanabe, K.; Taniguchi, T.; Novoselov, K. S.; Pey, K. L.; O'Shea, S. J. Dielectric Breakdown in Single-Crystal Hexagonal Boron Nitride. *ACS Appl. Electron. Mater.* **2021**, *3*, 3547−3554.
(55) Li, J.; Cao, X. K.; Hoffman, T. B.; Edgar, J. H.; Lin, J. Y.; Jiang, H. X. Nature of exciton transitions in hexagonal boron nitride. *Appl. Phys. Lett.* **2016**, *108*, 122101.
(56) Matović, B.; Luković, J.; Nikolić, M.; Babić, B.; Stanković, N.; Jokić; Jelenković, B. Synthesis and characterization of nanocrystaline hexagonal boron nitride powders: XRD and luminescence properties. *Ceram. Int.* **2016**, *42*, 16655−16658.
(57) Paine, R. T.; Narula, C. K. Synthetic routes to boron nitride. *Chem. Rev.* **1990**, *90*, 73−91.
(58) Hod, O. Graphite and Hexagonal Boron-Nitride have the Same Interlayer Distance. Why? *J. Chem. Theory Comput.* **2012**, *8*, 1360.
(59) Lee, D.; Song, S. H. Ultra-thin ultraviolet cathodoluminescent device based on exfoliated hexagonal boron nitride. *RSC Adv.* **2017**, *7*, 7831.
(60) Balapure, A.; Nikhariya, Y.; Sriteja Boppudi, N. S.; Ganesan, R.; Ray Dutta, J. Highly Dispersed Nanocomposite of AgBr in g-C3N4 Matrix Exhibiting Efficient Antibacterial Effect on Drought-Resistant Pseudomonas putida under Dark and Light Conditions. *ACS Appl. Mater. Interfaces* **2020**, *12*, 21481−21493.
(61) *Handbook of X-ray Photoelectron Spectroscopy*; Moulder, J., Stickle, W., Sobol, P., Eds.; Illustrated, Physical Electronics Division, Perkin-Elmer Corporation: Minnesota, 1992.
(62) Marini, A.; García-González, P.; Rubio, A. First-Principles Description of Correlation Effects in Layered Materials. *Phys. Rev. Lett.* **2006**, *96*, 136404.
(63) Marom, N.; Bernstein, J.; Garel, J.; Tkatchenko, A.; Joselevich, E.; Kronik, L.; Hod, O. Stacking and Registry Effects in Layered Materials: The Case of Hexagonal Boron Nitride. *Phys. Rev. Lett.* **2010**, *105*, 046801.
(64) Wang, L.; Xu, L.; Sun, C.; Qian, Y. A general route for the convenient synthesis of crystalline hexagonal boron nitride micromesh at mild temperature. *J. Mater. Chem.* **2009**, *19*, 1989.
(65) Sainsbury, T.; Satti, A.; May, P.; Wang, Z.; McGovern, I.; Gun'ko, Y. K.; Coleman, J. Oxygen Radical Functionalization of Boron Nitride Nanosheets. *J. Am. Chem. Soc.* **2012**, *134*, 18758.
(66) Bhimanapati, G. R.; Kozuch, D.; Robinson, J. A. Large-scale synthesis and functionalization of hexagonal boron nitride nanosheets. *Nanoscale* **2014**, *6*, 11671−11675.
(67) Khorasani, E.; Frauenheim, T.; Aradi, B.; Deák, P. Identification of the Nitrogen Interstitial as Origin of the 3.1eV Photoluminescence Band in Hexagonal Boron Nitride. *Phys. Status Solidi B* **2021**, *258*, 2100031.
(68) Attaccalite, C.; Bockstedte, M.; Marini, A.; Rubio, A.; Wirtz, L. Coupling of excitons and defect states in boron-nitride nanostructures. *Phys. Rev. B: Condens. Matter Mater. Phys.* **2011**, *83*, 144115.
(69) Sajid, A.; Reimers, J. R.; Kobayashi, R.; Ford, M. J. Theoretical spectroscopy of the V_NN_B defect in hexagonal boron nitride. *Phys. Rev. B* **2020**, *102*, 144104.
(70) Sajid, A.; Ford, M. J.; Reimers, J. R. Single-photon emitters in hexagonal boron nitride: a review of progress. *Rep. Prog. Phys.* **2020**, *83*, 044501.
(71) Hamdi, H.; Thiering, G.; Bodrog, Z.; Ivády, V.; Gali, A. Stone−Wales defects in hexagonal boron nitride as ultraviolet emitters. *npj Comput. Mater.* **2020**, *6*, 178.
(72) Weston, L.; Wickramaratne, D.; Mackoit, M.; Alkauskas, A.; Van de Walle, C. G. Native point defects and impurities in hexagonal boron nitride. *Phys. Rev. B* **2018**, *97*, 214104.
(73) Tsushima, E.; Tsujimura, T.; Uchino, T. Enhancement of the deep-level emission and its chemical origin in hexagonal boron nitride. *Appl. Phys. Lett.* **2018**, *113*, 031903.
(74) *Luminescence of Solids*; Gribkovskii, V. P., Vij, V. R., Eds.; Springer US: New York, 1998.
(75) Reich, S.; Ferrari, A. C.; Arenal, R.; Loiseau, A.; Bello, I.; Robertson, J. Resonant Raman scattering in cubic and hexagonal boron nitride. *Phys. Rev. B: Condens. Matter Mater. Phys.* **2005**, *71*, 205201.
(76) Berzina, B.; Korsaks, V.; Trinkler, L.; Sarakovskis, A.; Grube, J.; Bellucci, S. Defect-induced blue luminescence of hexagonal boron nitride. *Diamond Relat. Mater.* **2016**, *68*, 131−137.
(77) Khatri, P.; Luxmoore, I. J.; Ramsay, A. J. Phonon sidebands of color centers in hexagonal boron nitride. *Phys. Rev. B* **2019**, *100*, 125305.

https://doi.org/10.1021/acsomega.2c02884
ACS Omega 2022, 7, 33926−33933